ELSEVIER

Surface Science 327 (1995) 9–16

surface science

Epitaxial oxide formation on Cr(110) films

A. Stierle, P. Bödeker, H. Zabel *

Ruhr-Universität Bochum, Fakultät für Physik und Astronomie, Institut für Experimentalphysik, Festkörperphysik, 44780 Bochum, Germany

Received 17 October 1994; accepted for publication 12 December 1994

Abstract

We have investigated the oxidation of Cr(110) at 330°C and high oxygen exposures by surface sensitive X-ray scattering. Single crystal Cr(110) films prepared by molecular beam epitaxy (MBE) were used. Via in-situ X-ray reflectivity measurements the exact oxide thickness could be determined. New information about the metal/oxide interface was obtained: the oxidation is proceeding without roughening of the interface and the Cr(110) layers are oxidized in a layer-by-layer fashion. The number of Cr(110) planes can be counted before and after oxidation from in-situ Laue oscillation measurements of the Cr(110) Bragg peak. This reveals detailed information about the material consumption by the oxidation process. Additional ex-situ in-plane Bragg scans under grazing incidence show that an epitaxial, orthorhombic Cr_2O_3 layer in (0001) orientation is formed. The in-plane structure of the oxide layer can be improved by annealing in ultra-high vacuum.

Keywords: Chromium; Chromium oxides; Corrosion; Epitaxy; Metal–semiconductor interfaces; Molecular beam epitaxy; Oxidation; Single crystal epitaxy; X-ray scattering, diffraction, and reflection

1. Introduction

The oxidation of Cr(110) bulk single crystal surfaces has attracted much interest in the past because of its fundamental and application related importance [1]. Recently a new application of thin Cr_2O_3 oxide films has been demonstrated: they can be used as model systems for the analysis of catalytic reactions at solid state surfaces [2].

The dissociative oxygen chemisorption at room temperature has been described by different authors [3–6]. After room temperature adsorption and heating to higher temperatures (200–400°C) the formation of (100) facets on the Cr(110) surface is observed [3,5,7]. A facetting of the Cr(110) surface can also be observed during the homoepitaxial growth of Cr on Cr(110) [8,9], which is a general property of bcc metals. In the latter case the facetting is a kinetic process, which can be reversed by annealing to higher temperatures than the growth temperature, whereas the oxygen induced facetting is irreversible.

The oxidation at higher temperatures leads to the formation of an epitaxial Cr_2O_3 overlayer [7,10–12]. The structure of the oxide layer is supposed to be rhombohedrical in the (0001) orientation [7,10–12]. In addition, a spinel-type structure in the (111) orientation has been reported by Watari and Cowley [10].

The oxidation process itself has been studied with spectroscopic methods but is not very well understood up to now. The oxide growth law on Cr(110) has been investigated by several authors [1,4,5], however, leaving open a detailed, microscopic description of the oxidation process as a function of time and temperature. In particular, the exact oxide

* Corresponding author.

0039-6028/95/$09.50 © 1995 Elsevier Science B.V. All rights reserved
SSDI 0039-6028(94)00830-2

film thickness and the relation of the oxide microstructure to the oxidation behaviour have not been determined so far. It has been proved by tracer experiments [1] that the Cr ions move during the oxidation; it is not clear yet what kind of structural defects are responsible for the mass transport of the Cr ions in order to form a single crystalline oxide layer on top of the metal Cr(110) surface.

In this work thin single crystal Cr films were used to study the oxidation process. This has advantages over bulk Cr samples as concerns the preparation of a clean surface as well as for an exact account of the number of consumed metal atomic planes upon oxide formation. The oxidation was carried out at 330°C and at comparatively large oxygen exposures. We will present new results about the perpendicular structure of the Cr oxide/Cr system obtained by surface sensitive X-ray scattering experiments.

Surface sensitive X-ray scattering (together with surface sensitive neutron scattering) is the method of choice to determine the structure of layered systems in a non-destructive way [13–16]. We have demonstrated the power of X-ray reflectivity measurements for studying oxidation processes in the case of the oxidation of epitaxial Fe films with and without protective Au cap layers [17]. The oxide film thickness can be directly extracted from the specularly reflected intensity as a function of the scattering vector $\boldsymbol{K}$. The surface and interface roughnesses, i.e. the average fluctuations about an ideal interface, are obtained from a detailed analysis via a fit to the data. Moreover, the structural modifications of the surface by the oxidation can be followed on an atomic scale and the number of Cr(110) monolayers that have reacted with oxygen are counted by taking radial scans up to the first-order Bragg peak of the metal film.

In addition, in-plane Bragg reflections are measured under glancing incident angles to determine the in-plane crystallographic structure of the oxide layer before and after each annealing step. Information about the average crystallite size and mosaic distribution of the crystallites with respect to preferential orientations can be determined. The epitaxial relationship between the oxide and the underlying Cr layer is measured and compared to the results obtained with other surface sensitive methods.

2. Experimental

We have prepared single crystal Cr(110) films by molecular beam epitaxy (MBE) on a Nb(110)/

Fig. 1. 1×1 LEED pattern of a 25 nm thick Cr(110) film surface taken at 67 eV. The bulk lattice $[1\bar{1}0]$ direction is perpendicular to the long side of the rectangle formed by the spots; the bulk [001] direction stays normal to the short side.

$Al_2O_3(11\bar{2}0)$ buffer system as described in Ref. [18]. In this way we achieve atomically flat, clean Cr(110) surfaces without long annealing or preparation procedures. Typical film thicknesses are ranged from 10 to 100 nm. A representative low energy electron diffraction (LEED) picture of the Cr(110) film surface is reproduced in Fig. 1. It was taken at 67 eV and shows the diffraction pattern of an unreconstructed clean Cr(110) surface.

For the in-situ X-ray measurements the sample was transferred under UHV conditions from the MBE machine to an X-ray chamber equipped with beryllium windows and a furnace. The base pressure of this chamber was $< 10^{-9}$ Torr and it was pumped out continuously during the transport to the X-ray diffractometer by an accu-supplied ion pump. During heating and oxygen supply the chamber was pumped by a turbo-molecular pump. The temperature was controlled by a PtRh/Pt thermocouple placed directly behind the sample holder and it was cross-checked by measuring the thermal expansion of the sapphire substrate.

In fact, the oxidation was carried out under dynamical conditions; the oxygen inlet was adjusted to 5×10^{-5} Torr in the chamber while evacuating at the same time with a turbo-pump. In the present experiment the oxidation temperature was kept constant at 330°C.

The X-ray reflectivity measurements have been performed with a high resolution two circle diffractometer as described in Ref. [19], using Mo $K\alpha_1$ radiation with $\lambda = 0.070926$ nm. A 2 kW standard X-ray tube and a Si(110) monochromator were used. The maximum radial resolution is $\Delta K/K = 3 \times 10^{-4}$. In all measurements the scattering vector is oriented perpendicular to the physical surface of the sample or its lattice planes which differ slightly because of some arbitrary miscut of the substrate [19].

In general, reflectivity measurements are sensitive to optical properties like the refractive index and absorption of the material in the X-ray regime. The refractive index n is related via

$$n = 1 - \frac{2\pi r_0 \rho_e}{k_0^2} \tag{1}$$

to the electron density ρ_e of the material, neglecting dispersion corrections [20]. Here r_0 denotes the classical electron radius and k_0 the magnitude of the wave vector. Because of different electron densities from one material to the next, interference of the reflected waves can occur and the interference pattern depends strongly on the respective layer thicknesses and the roughness at each interface.

Using a recursive form of the Fresnel formulas including each interface, the reflected intensity can be calculated and compared to the experimental data [21]. This procedure is referred to as the Parratt formalism. All dispersion and absorption corrections to Eq. (1) are included and an additional term is taken into account to include the roughness at each interface according to Névot and Croce [22]. The result is an electron density profile of the system normal to the surface. The reliability and sensitivity of this technique in solving the structure of layered systems has been shown for many examples [23] and we have demonstrated it recently as well in the case of the oxidation of iron films [17].

To determine the crystallographic out-of-plane structure of the Cr films we scan the Cr(110) Bragg reflection. Because the film consists of a finite number of atomic planes in addition to the "normal" Bragg peak Laue oscillations on both sides of the Bragg reflection emerge. From the position of the main peak we determine the interplanar separation of the (110) planes. The separation of the Laue oscillations is a measure of the number of coherently scattering atomic (110) planes. The diffracted intensity can be calculated in usual kinematical approximation [20]:

$$I \propto \left| \sum_{l=0}^{N-1} e^{iKld} \right|^2 = \frac{\sin^2(NKd/2)}{\sin^2(Kd/2)}. \tag{2}$$

$K = 2k_0 \sin \vartheta$ is the magnitude of the scattering vector (ϑ is half of the scattering angle), d the distance of the Cr(110) planes and N the number of coherently scattering planes.

In the actual fit to the data points we include a Gaussian distribution of the number of coherently scattering planes because the measurement takes an average over macroscopic sample dimensions. Thus we will, in general, talk about the average number of coherently scattering planes $\langle N \rangle$ and its standard deviation ΔN. ΔN can be interpreted as an average lattice roughness [19], which can be compared to the

film roughness as determined by reflectivity measurements.

3. Oxidation of Cr(110)

In Fig. 2a we show the reflectivity of a 25 nm thick Cr(110) film deposited on a 20 nm thick Nb(110) buffer layer on an $Al_2O_3(11\bar{2}0)$ substrate. The reflected intensity (dots) is plotted as a function of the magnitude of the scattering vector K. Scan (1) was taken under UHV conditions at room temperature after sample preparation and transfer to the X-ray chamber. At $K = 0.536$ nm^{-1} the edge of total external reflection can be recognized followed by many finite film thickness oscillations. The average oscillation periodicity $\Delta K = 0.13$ nm^{-1} is approximately proportional to the inverse thickness D of the layers: $\Delta K = 2\pi/D$. Since the electron densities of the Nb and Cr layers are almost identical, ΔK measures the total thickness $D_{Nb} + D_{Cr}$, which is estimated to be 48 nm. The small amplitude modulation is due to the slight difference of their electron densities.

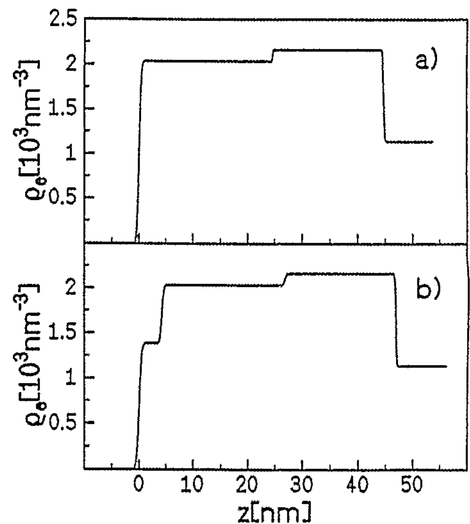

Fig. 3. The electron density is plotted as a function of the normal distance z from the surface. The profiles are used for the fits in Fig. 2. (a) A 24.7 nm Cr layer was deposited on top of a 20 nm Nb buffer layer. (b) After oxidation the Cr thickness is reduced to 22.2 nm and a 4.4 nm thin oxide layer is formed. The Nb layer thickness stays constant.

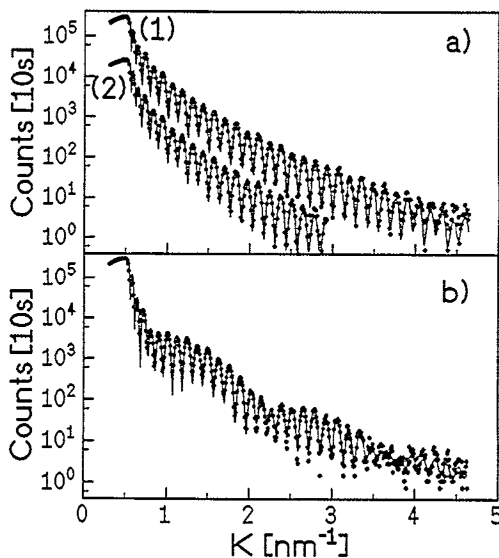

Fig. 2. Reflected intensity (dots) as a function of the magnitude of the scattering vector K. The solid lines are fits to the data points according to the electron density profiles plotted in Fig. 3. Curve (a) (1) is taken after UHV transfer of the sample from the MBE machine to the X-ray chamber and (2) during heating to 330°C. (b) Reflected intensity after oxidation at 330°C at $p_{O_2} = 5 \times 10^{-5}$ Torr for 1000 s. A long period intensity modulation occurs, which is attributed to the growing oxide layer.

The solid line is a fit to the data points using the Parratt formalism as described above. The diffuse, non-specular component was found to be less than 1% over the whole K spectrum measured here and could therefore safely be neglected.

The model of the electron density profile used for the fit is presented in Fig. 3a; the electron density is plotted as a function of the normal distance z from the surface. The smooth surface ($\sigma = 0.4$ nm) is followed by a 24.7 nm Cr layer and a 20 nm Nb layer on top of the infinite Al_2O_3 substrate. It should be noted, that the resulting electron densities of the metal films correspond to their respective bulk values. This is another indication for the high structural quality of the MBE films.

Fig. 4a shows a radial scan through the out-of-plane Cr(110) Bragg peak. The maximum peak position corresponds to the Cr(110) peak with lattice spacing of $d = 0.20357$ nm, which is close to the bulk value [18]. In addition, on both sides of the main Bragg peak Laue oscillations can be recognized, due to the finite number of Cr(110) lattice planes as described by Eq. (2). The slight asymmetry

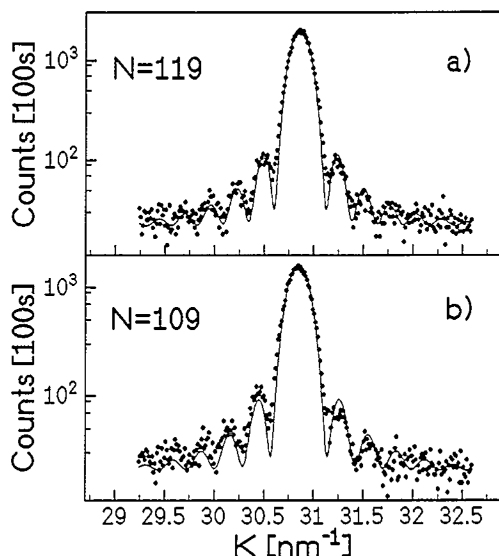

Fig. 4. Radial Bragg scans through the Cr(110) reflection (a) before and (b) after oxidation. The dots are the data points and the solid line is a fit according to the model described in the text. Before the oxidation the Cr film consists of 119 atomic planes, afterwards 109 planes are remaining. The transversal width of the Cr(110) reflection both before and after heating and oxidation is found to be $\Delta\Omega = 0.5°$.

between the left and right side of the Laue oscillation originates from interference effects between the Cr(110) Laue function, the crystal truncation rod (CTR) of the sapphire substrate and the Nb buffer layer Laue function. The Bragg peaks of both, the buffer and the substrate, are located at smaller K values. The asymmetry is neglected in the quantitative analysis.

The solid line is a fit to the data points using $\langle N \rangle = 119$ for the average number of coherently scattering lattice planes and $\Delta N = 4$ planes (~ 0.8 nm) for the standard deviation. The average coherent Cr film thickness follows from $D_{\mathrm{cohCr}} = \langle N \rangle \times d_{(110)} = 24.2$ nm and is in excellent agreement with the total Cr film thickness determined from the reflectivity measurement. This shows that the entire Cr film consists of flat and parallel Cr(110) planes, which is the essence of a single crystal film. The structural roughness $\Delta N = 0.8$ nm is larger than the Cr surface roughness determined from the reflectivity measurement ($\sigma = 0.4$ nm). This is reasonable because to the structural roughness fluctuations in N both at the surface of the Cr layer and at the Cr/Nb interface contribute. In addition a different property is measured because structural defects at the surface or the interface will affect the structural roughness, whereas the reflectivity roughness is unaffected.

In a second step the sample was heated to 330°C and the reflectivity measurement was repeated to ensure that no reaction with residual gas occurred. The result is plotted in Fig. 2a as scan (2), which is offset by a factor of ten for clarity. The reflectivity is very similar to the first measured at room temperature, confirming the stability of the sample.

The oxidation was carried out at an oxygen partial pressure of $p_{O_2} = 5 \times 10^{-5}$ Torr at 330°C. In this pressure range the rate of oxidation is limited by the system itself and not by the supply of oxygen from the gas phase [24]. The oxidation was monitored by the change of the reflected intensity at a fixed K value above the edge of total reflection. Within the first 10 s a very large drop of the reflected intensity was observed. During the following 1000 s only a very small intensity change was detected indicative for a very slow increase of the oxide layer thickness. In a forthcoming paper we will give a detailed account on the reflected intensity as a function of the oxidation time providing direct information on the growth law $L(t)$ of the oxide thickness L as a function of the oxidation time t. However, here we focus on the structural properties of the oxide layer.

After pumping off the oxygen and cooling down to room temperature, the reflectivity measurement, plotted as dots in Fig. 2b, reveals a dramatic change. In addition to the short period oscillations arising from the total thickness of the system a long period oscillation is superimposed with $\Delta K = 1.428$ nm^{-1}. This corresponds to a thickness of 4.4 nm in real space that can be attributed to the Cr oxide layer at the surface. From the fit to the data points (solid line) detailed information can be obtained: The electron density profile in Fig. 3b consists of a 4.4 nm thick oxide layer with a roughness of 0.5 nm. The electron density of the oxide layer can be determined to 1.38×10^3 nm^{-3} which is smaller than the Cr_2O_3 bulk value. The thickness of the underlying Cr layer has shrunk from 24.7 to 22.6 nm and its roughness of 0.4 nm stayed constant. This confirms the stability of the Cr_2O_3/Cr interface during the oxidation process and homogeneous oxide film formation.

The reduced Cr film thickness after oxidation should also be recognizable by scanning the Cr(110) Bragg peak because the number $\langle N \rangle$ of coherently scattering Cr(110) planes should be smaller after oxidation. In Fig. 4b the radial Bragg scan through the Cr(110) Bragg peak is plotted and the solid line is a fit according to Eq. (2) using an average number $\langle N \rangle = 109$ of coherently scattering lattice planes with $\Delta N = 4$ planes. The coherent film thickness $\langle N \rangle \times d_{(110)} = 22.2$ nm is essentially identical to the Cr film thickness deduced from the reflectivity data. Furthermore the structural roughness before and after oxidation agree with each other, which is another proof of the Cr/Cr_2O_3 interface stability during the oxidation.

To determine the in-plane structure of the oxide we performed in-plane Bragg measurements under grazing incidence with Cu Kα radiation ($\lambda = 0.15405$ nm). We used a 15 kW rotating anode system and a graphite monochromator. For the incoming beam the incident angle α_i was kept constant and equal to the critical angle for total external reflection from the surface. This induces an evanescent wave parallel to the sample surface [25]. The evanescent wave can be used to excite Bragg reflections from atomic planes *perpendicular* to the surface [26,27]. The Bragg reflected wave can be detected after being transmitted back through the surface. The out-coming wave has a specific dependence on the angle α_f relative to the surface giving an intensity maximum at the critical exit angle. In the present experiment the incident angle α_i was well defined and the exit angle was integrated over. This leads, in general, to a loss in surface sensitivity but in our case of an approximately 4 nm thick oxide layer the surface sensitivity is given by the thickness of the system itself. For a detailed description of the surface diffractometer setup used we refer to Ref. [28].

All surface diffraction experiments were carried out under normal atmospheric conditions after oxidizing the sample under the conditions described above. The overall structure of the oxide layer seemed to be stable under atmospheric conditions; reflectivity measurements indicate only a small increase in surface roughness originating possibly from the formation of carbonylic species at the surface.

Fig. 5a shows the intensity of the $Cr_2O_3(11\bar{2}0)$ Bragg peak as a function of the sample rotation angle ω from 0° to 180° (dots). The scattering vector is kept constant at the value of the bulk orthorhombic Cr_2O_3 $(11\bar{2}0)$ Bragg peak and the sample is rotated around the ω-axis oriented normal to the surface. Three peaks with a distance of 60° can be clearly identified indicating a sixfold symmetry in the plane, i.e. the whole lattice will have at least a threefold symmetry relative to the surface normal. The same measurements (not shown here) have been carried out keeping the scattering vector constant at the $Cr_2O_3(3\bar{3}00)$ reflection. Here again a sixfold in-plane symmetry can be recognized. Both measurements indicate that the oxide is orthorhombic α-Cr_2O_3 oriented with the (0001) axis parallel to the Cr(110) axis and its basal plane parallel to the Cr(110) plane in agreement with the results of other

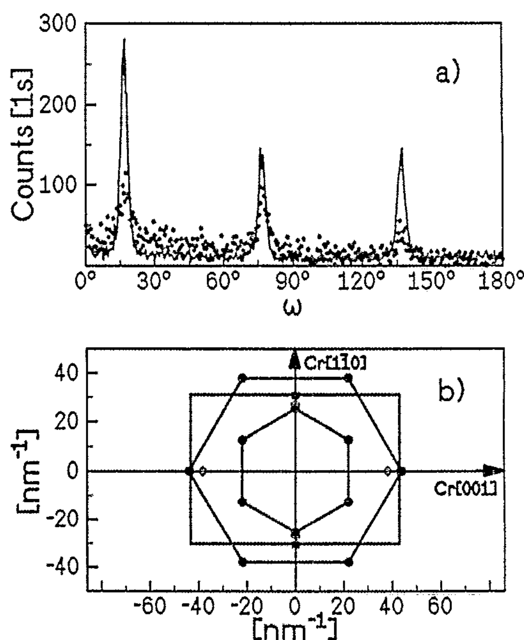

Fig. 5. (a) ω-scans with K fixed to the orthorhombic $Cr_2O_3(11\bar{2}0)$ reflection. Dots represent the scan taken directly after oxidation and the solid line the scan of the same sample post-oxidation heated to 550° in UHV. In both cases the reflections are separated by 60°, indicating a sixfold in-plane symmetry but after heating the reflected intensity increases and the reflections sharpen. (b) All in-plane reflections that were found, are collected in an in-plane reciprocal lattice. (◇) Nb reflections; (■) Cr reflections; (●) Cr_2O_3 reflections. Each of the six Cr_2O_3 $(11\bar{2}0)$ and $(3\bar{3}00)$ reflections lay on a hexagon. The hexagons are rotated 30° with respect to each other.

authors at different temperatures and oxygen exposures [7,10–12].

In Fig. 5a (solid line) is shown the same ω-scan however taken after annealing the sample at 550°C in UHV. Subsequent reflectivity measurements (not shown here) confirmed, that the oxide thickness has not changed during the anneal. The in-plane ω-scan reveals again three peaks separated by 60°, but the peak height has increased and the peaks have become sharper as before. This indicates a dramatic increase in lateral structural order; the defect density is reduced and the oxide crystallites grow in size. The average in-plane mosaic distribution has changed from $\Delta\omega = 5.1°$ to $\Delta\omega = 3.7°$.

Fig. 5b summarizes the in-plane information for the whole system via the in-plane reciprocal lattices of Cr, Cr_2O_3 and Nb as determined from in-plane Bragg diffraction. The filled circles denote the Cr-oxide Bragg peaks; open diamond-shaped symbols and filled squares represent Nb and Cr reflections, respectively. The epitaxy of Cr(110) on Nb(110) is described elsewhere [18]; here the interest is focused on the oxide: the $Cr_2O_3[11\bar{2}0]$ direction is oriented parallel to the $Cr[1\bar{1}0]$ direction and the $Cr_2O_3[1\bar{1}00]$ direction is parallel to the Cr[001] direction. The good epitaxy between the oxide and the Cr(110) surface is manifested in the Cr[001] direction: the misfit between the oxide and the metal is less than 0.5% and the Cr(002) and $Cr_2O_3(3\bar{3}00)$ lattice plane distances are nearly identical.

4. Conclusions

We have demonstrated the power of epitaxial metal films for the study of surface reaction processes. In this case we studied the oxidation of Cr(110) films. Reflectivity measurements and radial Bragg scans reveal a layer-by-layer growth of the Cr oxide without roughening of the metal/oxide interface at 330°C. This is in contrast, e.g., to the oxidation of Ni(100) at room temperature where an island-like oxide growth with large tilting of the oxide lattice with respect to the metal surface is reported [29].

At 330°C the formation of a 4.4 nm oxide film consumes exactly 10 Cr(110) lattice planes. Assuming the formation of a defect-free, stochiometric and orthorhombic Cr_2O_3 layer ($a = 0.4954$ nm, $c = 1.3584$ nm, $\rho_e = 1.507 \times 10^3$ nm^{-3}) from the oxidation of 10 Cr(110) layers, then 3 Cr_2O_3 unit cells in the (0001) direction can be built up. This corresponds to an oxide thickness of 4.1 nm, which is in good agreement with the measured value of 4.4 nm. In fact, the deviation to higher thicknesses can be explained in the following way: from the fit to the reflectivity curve (Figs. 2b and 3b) the electron density of the oxide layer can be determined to $\rho_e = 1.38 \times 10^3$ nm^{-3} within experimental errors. This value is smaller than the bulk value by the same amount as the measured oxide film thickness is expanded compared to bulk Cr_2O_3. Consequently, Cr defects must be present, reducing the total electron density of the system. The Cr ions are distributed in a larger volume resulting in an increase of the oxide film thickness, as observed. The Cr defects are supposed to serve as oxidation promotors.

In the plane, the oxide forms an ordered epitaxial structure on top of the Cr(110) film with sixfold in-plane symmetry. The in-plane lattice parameters are in good agreement with the bulk values of rhombohedrical Cr_2O_3. A small isotropic deviation (+0.5%) to larger lattice spacings is due to the epitaxial strain in the $Cr_2O_3(1\bar{1}00)$ direction. After annealing to 550°C in UHV the oxide does not decompose; instead the lateral structure of the oxide is improved and in-plane defects are removed. Here only a redistribution of atoms in the plane seems to occur. The annealing step has no influence on the oxide thickness and it does not increase the electron density of the oxide layer as can be seen from reflectivity measurements, which are not shown here. Because of this, we conclude that the defects observed by the reflectivity measurements are not identical to the in-plane defects, the latter being removed by annealing. Instead we propose the existence of out-of-plane defects like stacking faults of subsequent layers. The out-of-plane structure of the oxide layers and its relation to the oxidation behaviour at different temperatures will be investigated in future work by crystal truncation rod (CTR) measurements.

Acknowledgments

We would like to thank Professor H.-J. Freund and Dr. H. Kuhlenbeck for fruitful discussions. This

work was supported by the Deutsche Forschungsgemeinschaft within the Graduiertenkolleg "Dynamische Prozesse an Festkörperoberflächen".

References

[1] A. Atkinson, Rev. Mod. Phys. 57 (1985) 437.
[2] C. Xu, M. Hassel, H. Kuhlenbeck and H.-J. Freund, Surf. Sci. 258 (1991) 23.
[3] N.D. Shinn and T.E. Madley, Surf. Sci. 173 (1986) 379.
[4] Y. Sakisaka, H. Kato and M. Onchi, Surf. Sci. 120 (1982) 150.
[5] J.S. Foord and R.M. Lambert, Surf. Sci. 161 (1985) 513.
[6] A.G. Baca, L.E. Klebanoff, M.A. Schulz, E. Paparazzo and D.A. Shirley, Surf. Sci. 173 (1986) 215.
[7] H.M. Kennett and A.E. Lee, Surf. Sci. 33 (1972) 377.
[8] M. Albrecht, H. Fritzsche and U. Gradmann, Surf. Sci. 294 (1993) 1.
[9] W. Donner, unpublished.
[10] F. Watari and J.M. Cowley, Surf. Sci. 105 (1981) 240.
[11] P. Michel and Ch. Jardin, Surf. Sci. 36 (1973) 478.
[12] S. Ekelund and C. Leygraf, Surf. Sci. 40 (1973) 179.
[13] H. Zabel, in: Festkörperprobleme, Advances in Solid State Physics, Vol. 30, Ed. U. Rössler (Vieweg, Braunschweig 1990) p. 197.
[14] H. Zabel, Appl. Phys. A 58 (1994) 159.
[15] R. Feidenhans'l, Surf. Sci. Rep. 10 (1989) 105.
[16] I.K. Robinson and D.J. Tweet, Rep. Prog. Phys. 55 (1992) 599.
[17] A. Stierle, T. Mühge and H. Zabel, J. Mater. Res. 9 (1994) 884.
[18] P. Sonntag, W. Donner, N. Metoki and H. Zabel, Phys. Rev. B 49 (1994) 2869.
[19] A. Stierle, A. Abromeit, N. Metoki and H. Zabel, J. Appl. Phys. 73 (1993) 4808.
[20] B.E. Warren, X-Ray Diffraction (Addison-Wesley, Reading, 1969).
[21] L.G. Parratt, Phys. Rev. 95 (1954) 359.
[22] L. Névot and P. Croce, Rev. Phys. Appl. 15 (1980) 761.
[23] H.J. Lauter and V.V. Pasyuk, Eds., Proceedings of the International Conference on Surface X-ray and Neutron Scattering SXNS-3, Physica B 198 (1994).
[24] A.T. Fromhold and E.L. Cook, Phys. Rev. 158 (1967) 600.
[25] J. Als Nielsen, in: Structure and Dynamics of Surfaces II, Topics in Current Physics, Vol. 43, Eds. W. Schommers and P. Blanckenhagen (1987).
[26] H. Dosch, Phys. Rev. B 35 (1987) 2137.
[27] H. Dosch, Critical Phenomena at Surfaces and Interfaces, Springer Tracts in Modern Physics, Vol. 126 (Springer, Berlin, 1992).
[28] N. Metoki, W. Donner and H. Zabel, Phys. Rev. B 49 (1994) 17351.
[29] M. Bäumer, D. Cappus, H. Kuhlenbeck, H.J. Freund, G. Wilhelmi, A. Brodde and H. Neddermeyer, Surf. Sci. 253 (1991) 116.